Enlightening the effect of Strontium in the $BiVO_4$-TiO_2 diphase composites for dielectric devices

K. Yukesh Kumar[a], N. Sivakumar[a,], G.M. Bhalerao[b], G. Anbalagan[c], Kentaro Tashiro[d], Ali Alsulmi[e]

[a]Functional Materials Research Laboratory (FMRL), Department of Physics, Sri Sairam Engineering College, Chennai-600 044, Tamil Nadu, India.

[b]UGC-DAE Kalpakkam Node, Kokilamedu-603 104, Tamil Nadu, India.

[c]Department of Nuclear Physics, University of Madras, Chennai-600 025, Tamil Nadu, India.

[d]National Institute for Materials Science, Tsukuba-305-0044, Japan.

[e]Department of Chemistry, College of Science, King Saud University, Riyadh, Saudi Arabia.

*Corresponding Author

E-mail id: sivakumar.phy@sairam.edu.in

Abstract

$Bi_{(1-2/3x)}Sr_xVO_4$-TiO_2(x = 0, 0.1, 0.15) composite materials were prepared by the conventional solid state reaction method at optimized temperature of 750°C. The effect of Strontium (Sr) element in the stoichiometric system of $BiVO_4$-TiO_2 on structural phase, micro-morphology, elemental composition, band energy and dielectric properties were systematically analyzed for the first time. All the composite materials synthesized with different concentrations of Sr have two structural phases, monoclinic structure which belongs to $BiVO_4$ whereas tetragonal structure belongs to the rutile TiO_2. The relative dielectric permittivity (ε_r) gradually increased from ~ 61 to 122 with the increase of Sr concentration in the $Bi_{(1-2/3x)}Sr_xVO_4$-TiO_2(x = 0, 0.1, 0.15) composite. The temperature dependent ac electrical conductivity (σ_{ac}) of the prepared materials was estimated in the frequency range from 50 to 3 MHz. The microwave dielectric properties of the prepared composite materials are examined at 3.9 GHz and results were discussed in detail for their potential dielectric applications.

Keywords: Solid state reaction; Powder X-Ray Diffraction; Surface morphology; UV analysis; Dielectric constant; Microwave dielectrics

1. Introduction

In this modern era, owing to the drastic usage of cellular phones in day-to-day life, researchers are finding the new paths in the field of wireless communication technologies. The conversion of the microwaves as a carrier wave in the wireless communication technologies that have developed in the area of miniaturization of device fabrication has been a difficult task for the researchers. The dielectric oxide ceramic materials brought a drastic improvement in the wireless communication industries by reducing the size and cost of filters, dielectric resonators,

oscillators, and antennas for the application usage from cellular phones to global positioning systems (GPS). Also, the wireless communication technologies have their own special features and functions due to their reduced size and weight for the comfortable usage of mankind.

Generally, dielectric resonators are an electromagnetic component that shows resonance, which is used for the narrow range of frequencies. They exhibit high permittivity and low dissipation factor. These developments of dielectric resonators play an important role in modern wireless communication technologies. Additionally, the ceramic dielectric resonators have developed more miniaturized components than the traditional microwave materials and possess a high-quality factor. The ceramic dielectric resonators have some unique features like cost advantage, lesser dimension, less weight, stable and efficient device performance, tenability, and ruggedness. Also, the temperature variations of the resonant frequency have excellent output, which is a significant requirement for circuit designers. Dielectric resonator filters are generally used to differentiate the wanted frequency from most of the unwanted signal frequencies in the transmitter and receiver end. These potential dielectric resonators depend on the three major factors, such as high relative permittivity (ε_r), high quality factor (Q_f) and near-zero temperature coefficient of resonant frequency (TCF). The less permittivity dielectric materials are used in the field of millimeter wave communication, as well as for substrates in the development of microwave integrated circuits. The dielectric materials with permittivity in the range of 25–50 are used for the satellite communication and cellular base station. The dielectric materials of permittivity > 50 are used in the field of mobile phone manufacturing, particularly in the area of developing miniaturization [1].

Low-temperature co-fired ceramics (LTCC) is another important factor that plays a dominant role in developing an integrated microwave device in the modern communication system. In general, dielectric material is fired with an Ag electrode at the temperature below its melting point (961°C) for the development of cost-effective electrodes [2-4]. Some materials have significant microwave dielectric properties which are suitable for the LTCC technologies but they are limited due to their high sintering temperature. Bi-based oxides and V_2O_5 ceramic dielectric materials are effectively used for LTCC applications, which are sintered at a temperature below 900°C [5–10].

In this aspect, we have identified Bi_2O_3-V_2O_5 as a potential candidate for its dielectric applications, as they have significant properties like as paraelectricity, ferroelectric, conductivity, and ionic conductivity, as well as for its

acoustic-optical and photocatalytic applications [11–17]. In addition, it has a low sintering temperature, which suits for many LTCC device applications [18]. Also, the Bi_2O_3-V_2O_5 system has excellent microwave dielectric properties such as high relative permittivity (ε_r) ~68 and high quality factor (Q_f) ~ 6500, with a high negative value of temperature coefficient of resonant frequency (τ_f) in the range from -243 to -260 ppm/°C [19]. Jun Hong Noh et al. discussed the potential microwave dielectric properties of TiO_2, like high relative permittivity (ε_r) ~ 100 and quality factor (Q_f) ~ 14,000, with a high positive value of temperature coefficient of resonant frequency (τ_f) of +400 ppm/°C [20]. The addition of ZnO in Bi_2O_3-V_2O_5 shows high dielectric permittivity (ε_r) ~500 and loss ~ 101 at 100Hz frequency [21]. Chen et al. investigated the microwave dielectric properties of a $Li_{0.5}Re_{0.5}$-WO_4 system that has relative permittivity (ε_r) ~71.8 and quality factor (Q_f) ~ 7482 at low firing temperature below 800°C [22]. Oliveira et al. demonstrated the dielectric properties on the addition of TiO_2 in the Bi_2O_3 V_2O_5 system, which shows less dielectric constant (ε_r) ~38.2 as well as loss (Tanδ) ~ 7 x 10^{-2} [23].

In the present work, we prepared $BiVO_4$-TiO_2composite materials with the different Sr concentration at the A^+(Bi) site via the cost-effective solid-state synthesis method. Also the crystal structure, phase identification, microstructure features, chemical composition, dielectric and microwave dielectric parameters were systematically studied and compared the results of the Bi $_{(1-2/3x)}$ Sr_xVO_4-TiO_2(x = 0, 0.1, 0.15) composites for the first time.

2. Experiment

2.1. Preparation of Bi $_{(1-2/3x)}$ Sr_x VO_4-TiO_2 (x = 0, 0.1, 0.15) composite materials

A conventional solid state reaction technique was employed to synthesize the pure $BiVO_4$-TiO_2 (BVT) and Sr doped Bi $_{(1-2/3x)}$ Sr_xVO_4-TiO_2(x = 0.1, 0.15) composite materials. The dopant, Sr = 0.1 wt % and Sr = 0.15 wt % in the Bi $_{(1-2/3x)}$$Sr_xVO_4$-$TiO_2$(x = 0.1, 0.15) composite material were named as 1SBVT and 2SBVT respectively. The starting materials, Bismuth Oxide (Bi_2O_3), Vanadium Pentoxide (V_2O_5), Titanium Oxide (TiO_2) and Strontium Carbonate ($SrCO_3$) with high purity (99.9%) of fine powder are purchased commercially from sigma Aldrich. Initially the Bi_2O_3, V_2O_5 and TiO_2 were pre-heated to 500 ℃ for 6 hours and $SrCO_3$ pre-heated to 150 ℃ to avoid the absorption of foreign particles and activate the materials for the reaction process. The stoichiometric ratio of the reactant powders BVT were mixed, crushed and grinded well to get a fine powder with the support of mortar and pestle for 6 hours. The fine powders were then transferred into a crucible and calcinated at 750 ℃ for 6 hours, and

then bring back to room temperature using a box furnace. The calcinated powders were again grinded well with a mortar and pestle for about 5 hours to obtain a fine composite powder. The final powder was pressed into a circular disc shaped pellet with the dimension of 10 mm diameter and 5 mm thickness. The pellets were then sintered at 750 ºC for 4 hours. The same procedure was followed to prepare the 1SBVT and 2SBVT composite materials, respectively.

2.2. Characterization details

The powder X-ray diffraction was recorded in the 2θ region from 5º to 60º using XPERT-PRO X-Ray Diffractometer with Cu-Kα radiation (λ = 1.5406 Å) to identify the crystalline structure of the prepared composite materials. The surface morphology features and elemental compositions of the prepared materials were examined by the Scanning Electron Microscope system equipped with energy dispersive X-ray (EDX) setup. The elemental composition of the prepared composite materials was identified by Peek Seeker Raman Spectrophotometer recorded in the range from 100 to 1000 cm^{-1}. Spectral Studies were carried out to estimate an optical band gap value of the prepared composite material with JASCO V-760 Spectrophotometer, which was used to record the UV- visible spectrum in the region, 200 to 800 nm. The sintered pellets were coated with conducting silver paste on both the sides for the better electrical conductivity. The prepared pellets were subjected to HOIKI IM3536 LCR Meter impedance analyzer to study the electrical behaviors of the prepared composite materials. The prepared pellets were subjected to Microwave Vector Network Analyzers to study the microwave dielectric properties at 3.9 GHz. The TE_{001} mode was utilized to determine the dielectric constant. The temperature coefficient of resonant frequency, TCF (τ_f) was evaluated within a temperature range of 28–60°C. The TCF value was then calculated using the following formula,

$$\tau_f = \frac{f_{60} - f_{28}}{f_{28}(60-28)} \quad (1)$$

Where f_{60} and f_{28} are the resonant frequency at 60 °C and 28 °C, respectively

3. Results and discussion

3.1. Powder X-Ray Diffraction (PXRD) Analysis

The powder X-ray Diffraction patterns of the prepared composite materials of $Bi_{(1-2/3x)}Sr_xVO_4$-TiO_2(x = 0, 0.1, 0.15) are shown in Fig. 1. The prominent reflection peaks are observed at the Bragg's angles 2θ = 18.67º,

28.94º, 30.54º, 34.49º, 35.22º, 39.78º, 42.46º, 46.03º, 46.71º, 47.30º, 50.31º, 54.58º, 58.53º and 59.26º. The corresponding (h k l) planes are identified as (110), (121), (040), (200), (002), (211), (051), (132), (240), (042), (202), (013), (321) and (123) respectively. The identified planes are well-matched with the XRD patterns of JCPDS Card No.14-068, which belongs to the monoclinic structure of $BiVO_4$ with space group of I2/a. The remaining peaks around at 27.5º, 36.4º and 54.1º with (110), (101) and (211) respectively belongs to the tetragonal structure of rutile TiO_2 (JCPDS Card No. 21-1276) are well-matched with the previously reported XRD pattern of TiO_2 [24, 25]. The observation of two phases in the prepared materials is due to the formation of tetrahedral coordination site by the V^{5+} ions with ionic radius 0.355 Å. But Ti^{4+} naturally prefers to form the octahedral coordination sites. Due to the chemical and structural unstable nature of Ti^{4+}ions, they do not fit with the Tetrahedral sites of the V^{5+} of $BiVO_4$ [2]. Also, it is observed that the XRD peak intensities of Sr doped $BiVO_4$-TiO_2 materials are reduced when compared with the pure $BiVO_4$-TiO_2composite material. The reduction in XRD peak intensities is likely due to changes in crystallinity caused by the incorporation of Sr ions into the $BiVO_4$-TiO_2 structure. Scherer's equation [26] is used to calculate the average crystallite size D (nm) of the prepared composite materials.

$$D = \frac{k\lambda}{\beta cos\theta} \qquad (2)$$

where k is the Boltzmann constant, θ indicates the position of the diffraction peak, λ is the wavelength of the X-Ray source and β is the full width at half maximum (FWHM) of the peaks observed. The estimated crystallite size values of BVT, 1SBVT and 2SBVT are found to be 66 nm, 54 nm and 48 nm respectively. The average crystallite size of the prepared composite materials was found to decrease in size gradually from pure BVT to Sr doped BVT samples. The Williamson–Hall method has been utilized to analyze the broadening of XRD peaks, which is used to understand the size-induced and strain-induced molecular effects. This approach helps to determine the strain present in the synthesized composite materials. The Williamson–Hall equation can be expressed as:

$$\beta cos\theta = \frac{K\lambda}{D}\ 4\varepsilon\ sin\theta \qquad (3)$$

β represents the full width at half maximum (FWHM), λ is the X-ray wavelength (1.5406 Å), θ is the Bragg angle, kis a constant (0.9) referred to as the shape factor, D denotes the crystallite size, and ε represents the strain.

Figs. 2(a-c) illustrate the plots of βcosθ versus 4sinθ for the samples BVT, 1SBVT and 2SBVT. The linear fit of these plots are utilized to calculate the strain values. The estimated strain values are 1.63 x 10^{-4}, 2.01x 10^{-4} and 2.31x

10^{-4} for the samples BVT, 1SBVT and 2SBVT respectively. The increase in strain observed in $BiVO_4$-TiO_2 due to the addition of Sr which develops distortions in the crystal structure.

The bulk density was calculated by the Archimedes method for the prepared composite materials. The values were found to be 5.72 (g/cm^3), 5.94 (g/cm^3), and 6.03 (g/cm^3) for the samples BVT, 1SBVT and 2SBVT respectively. It is noted that the increase of density is owing to the addition of strontium in BVT system. The porosity of the prepared composite materials BVT, 1SBVT and 2SBVT were measured to be 7.53%, 2.04% and 1.97% respectively. The theoretical density of the for the prepared composite materials were calculated using the formula

$$\text{Theoretical density } (g/cm^3),\ \rho = \frac{Z.\ M}{N_A.V} \qquad (4)$$

where Z is the number of formula units per unit cell, M is the molar mass of the compound (g/mol), N_A = Avogadro's number (6.022×10^{23} atoms/mol) and V is the volume of the unit cell (cm^3). The values were found to be 6.50 (g/cm^3), 6.28 (g/cm^3), and 6.17 (g/cm^3) for the samples BVT, 1SBVT and 2SBVT respectively. Also, the relative density (g/cm^3) is calculated for the prepared composite materials by the formula

$$Relative\ density = \frac{Bulk\ Density}{Theoretical\ Density} \qquad (5)$$

The values were found to be 88%, 94.6% and 97.73%for the samples BVT, 1SBVT and 2SBVT respectively.

3.2. Scanning Electron Microscope with EDX Analysis

Figs. 3(a-c) show the surface and micro morphology features of the prepared composite materials of $Bi_{(1-2/3x)}Sr_xVO_4$-TiO_2 (x = 0, 0.1, 0.15). These images revealed that the prepared composite materials are agglomerated with irregular shapes containing small porous in-between the grains and surface shows two distinct grain colours. The white colour represents the $BiVO_4$ grains and the dark black colour indicates the rutile TiO_2 grains respectively [25]. Thus, the SEM study confirms the presence of two phases, as observed in the PXRD studies. Figs. 4(a-c) represent the histogram plots (plotted with ImageJ Software) of the $Bi_{(1-2/3x)}Sr_xVO_4$-TiO_2(x = 0, 0.1, 0.15) composite materials to estimate the average grain size. The average grain size values of pure $BiVO_4$-TiO_2, 0.1 wt% Sr doped and 0.15 wt% Sr doped $BiVO_4$-TiO_2 composite materials are determined to decrease in particle size (area) and the values are determined to be 1.43 μm, 1.35 μm, 1.09 μm respectively. It is found that the grain size decreases with the

increase of Sr doping concentration in $BiVO_4$-TiO_2, which is in analogous to the crystallite size decrement as observed from the PXRD results. Also, the Figs. 5(a-c) show the EDX micrograph of the composite products, which explains the presence of elemental compositions. In addition, Table 1 provides the detail of the weight percentage of the chemical elements in the prepared composite materials for further understanding.

3.3. FT-Raman Spectral analysis

Fig. 6 show the Raman spectrum of $Bi_{(1-2/3x)}Sr_xVO_4$-TiO_2(x = 0, 0.1, 0.15) composite materials. The corresponding Raman vibrational assignments are listed in Table 2. The Raman vibrational peak at 124 cm^{-1} corresponds to O-Ti-O bond [27]. A sharp peak at 208 cm^{-1} belongs to Bi-O bond [28-29]. The observed medium Raman band between 329 and 365 cm^{-1} corresponds to symmetrical bending of VO^{4+}[30]. A wide Raman band near 609 cm^{-1} attributed to stretching bond of O- Ti-O [27]. The high intensity Raman peak observed at 820 cm^{-1} represents the V-O Stretching bond [30]. The doping of Sr in the $BiVO_4$-TiO_2 composite system shows Raman peaks remind at the same position. So the fundamental vibrations of $BiVO_4$-TiO_2 system not altered by the Sr dopant.

3.4. UV – Vis. Spectral analysis

Fig. 7 describes the UV- Visible absorption details of the prepared composite materials $Bi_{(1-2/3x)}Sr_xVO_4$-TiO_2(x = 0, 0.1, 0.15) that are measured in the range 200 to 1000 nm. The lower cut off wavelength is observed for all the materials around at 430 nm, and no further absorption occurred in the visible region. A small absorption in the $BiVO_4$-TiO_2 system at 282 nm in the UV region is due to the $\pi \rightarrow \pi^*$ transition [31, 32]. All the Sr doped composite materials have the same absorption in the same position. Fig. 8 (a-c) explains the optical band gap details of pure $BiVO_4$-TiO_2 (BVT), 0.1 wt% Sr doped (1SBVT) and 0.15 wt% Sr doped $BiVO_4$-TiO_2 (2SBVT) composites respectively. The optical bandgap energy values of the prepared composite materials of BVT, 1SBVT and 2SBVT are calculated from the optical absorption coefficient (α) using an absorbance data using the relation,

$$\alpha = \frac{2.303}{d} \log \frac{1}{T} \qquad (6)$$

where T is the Transmittance and d is the thickness of the sample.

The relation between the optical absorption coefficient (α) and the photon energy (E= hυ) is given by,

$$\alpha h\upsilon = A(h\upsilon - E_g)^m \quad (7)$$

where A is the material's constant, h is the Planck's constant, υ is the optical frequency, E_g is the optical bandgap energy and 'm' is an index. The bandgap energy is calculated using the plot drawn between the (hν) vs. $(\alpha h\nu)^2$. The prepared composite material possesses a direct transition and the optical bandgap values are found to be 2.45 eV, 2.48 eV and 2.53 eV corresponds to BVT, 1SBVT and 2SBVT respectively. The strontium doped composite materials (1SBVT & 2SBVT) show slightly increased bandgap energy due to the quantum confinement effect. That is, when the crystallite size as well as particle size decreases, the bandgap energy increases.

3.5. Dielectric analysis

Particular composite materials are having unique properties such as microstructure and lower dielectric constant that find their usefulness in frequency response and AC conductivity for the development of the technological growth in various fields particularly in the fabrication of the resonators, antennas and filters for the application of mobile device and satellite broadcasting. The size requirements of electronic components are getting smaller and smaller in the latest wireless communication gadgets tends way to miniaturization and integration of the devices [22, 33-38]. Through the study of dielectric properties of the materials, we can explore more insights about the atomic dislocation and various polarization mechanisms which include electronic, ionic, orientation and space polarization for the device developments. Generally, the materials having high dielectric constant values tend to dissipate significant power when used for higher frequency application [39]. Figs. 9 (a-c) describe the dielectric constant and Figs. 10 (a-c) shows dielectric loss of the prepared composite materials. We studied the dielectric properties of the materials in the frequency range of 1 KHz – 3 MHz with various temperatures starting from room temperature to 70°C in the steps of 10ºC. It is observed that the gradual decrease in the dielectric constant of the prepared composite materials with the increase of frequency and stabilizes at higher frequencies. Initial higher dielectric constant at the lower frequency range is attributed to the electrode interface effect. Local electronic displacement within the materials creates polarization that occurs along the direction of the applied field. However, at higher frequencies, the molecular dipoles do not respond to the applied electric field. These various polarizations lead to the decrease in the dielectric constant until it becomes stabilized at the higher frequencies [40]. The dielectric constant (ε_r) of the materials is calculated using the relation,

$$\varepsilon_r = \frac{C_p}{\varepsilon_0}\frac{d}{A} \quad (8)$$

where C_p is the capacitance in parallel, ε_o is the permittivity of free space, A is the area of the sample surface and d is the thickness of the sample. The dielectric constant (ε_r) of the prepared composite sample are found to be ~61, ~95 and ~120 corresponding to BVT, 1SBVT and 2SBVT composites respectively. The mentioned dielectric values are recorded at the frequency of 3MHz with temperatures RT, 50℃, 60℃, and 70℃. The increase in dielectric constant with the increase of addition of strontium in $BiVO_4 - TiO_2$ is due the increase in strain, reduced crystallite size which gradually increases the polarization. The dielectric constant values calculated for all the samples at different temperature shows small variation with the rise of temperature. This is due to the fact that the thermal excitation energy by the bound charge carriers, which gradually increases the polarization that leads to the increase in the dielectric constant [41].

The dielectric loss values of the prepared ceramic material are found to be 0.025, 0.195 and 0.047 which are recorded at frequency 3MHz corresponding to the BVT, 1SBVT and 2SBVT composites respectively. The loss factor gradually increases with the addition of the strontium leads to increase in conductive behavior due to the relaxation of the charges at grain boundaries.

The ac electric conductivity (σ_{ac}) has been calculated by the relation

$$\sigma_{ac} = \omega\, \varepsilon_o\, \varepsilon_r\, \mathrm{Tan}\, \delta \quad (9)$$

where ω is the angular frequency ($2\pi f$), Tan δ is the loss factor. The graph is plotted against the function of log *f* and ac electric conductivity (σ_{ac}) for various temperatures with the frequency range of 1 KHz to 3 MHz are shown in the Figs. 11 (a-c). The conductivity of the prepared composite materials is 8.9×10^{-5}, 7.6×10^{-4}, 3.5×10^{-4} $S.m^{-1}$ recorded at frequency 3MHz corresponding to BVT, 1SBVT and 2SBVT composites respectively. The conductivity follows the equation given by

$$\sigma(\omega) = \sigma_{dc} + P\, \omega^{\eta} \quad (10)$$

The above equation is the Johscher's power law (42) where $\sigma_{dc}$is the dc conductivity and η is the exponent of a power law which represents the mobile ions which measures the interaction of charge carriers along with the lattice. The conductivity versus frequency spectrum (Fig. 11) shows the increase of ac-conductivity with frequency.

This increase in ac-conductivity with higher frequency and temperature supports the negative temperature coefficient of resistance (NTCR) behavior of the synthesized sample. The variation in conductivity of ($Bi_{(1-2/3x)}Sr_xVO_4$-TiO_2 (x = 0, 0.1, 0.15) with the inverse of the absolute temperature at different frequencies are presented in Fig 12(a-c). The ac-conductivity can be calculated by using the equation

$$\sigma_{ac} = \sigma_0 \exp\left(\frac{Ea}{kT}\right) \quad (11)$$

where k and σ_0 are the Boltzmann constant and the pre-exponential factor, respectively. The activation energy E_a can be calculated with the slope using the relation, E_a = -2.303 × slope × 1000 X k. The activation energy of the prepared polycrystalline material of BVT is 0.0134eV, 0.0184eV and 0.0033eV at frequencies 1 KHz, 100 KHz and 1 MHz respectively. Also for 1SBVT composite is 0.0127eV, 0.0159eV and 0.002eV at frequencies 1 KHz, 100 KHz and 1 MHz respectively and for 2SBVT is 0.0156eV, 0.0756eV and 0.00154eV at frequencies 1 KHz, 100 KHz and 1 MHz respectively. The low activation energy in metal oxides used in dielectric studies indicates that the material is likely to demonstrate favorable dielectric properties with minimal energy barriers for charge movement or dipole orientation. This phenomenon revealed that the prepared materials are well-suited for various applications such as capacitors, sensors, and other electronic devices.

3.6. Microwave dielectric properties analysis

Fig. 13 show the microwave dielectric permittivity and temperature coefficient resonant frequency (τ_f) of the prepared composite materials ($Bi_{(1-2/3x)}Sr_xVO_4$-TiO_2 (x = 0, 0.1, 0.15). Fig. 14 shows the quality factor of the prepared composite materials ($Bi_{(1-2/3x)}Sr_xVO_4$-TiO_2 (x = 0, 0.1, 0.15). The measured values of microwave dielectric permittivity (ε_r) at 3.9 GHz are 68, 73, and 77 which correspond to the BVT, 1SBVT and 2SBVT composites respectively. The ε_r increases with the increase in strontium content. In this constant, the dielectric permittivity (ε_r) is depended upon the density, ionic polarizability, secondary phase, etc. [43]. This enhancement in permittivity is mainly attributed to the higher polarizability introduced by strontium doping, which modifies the crystal lattice structure. The quality factor (Q_f) value of ceramics can be affected by intrinsic factors (such as vibration modes and packing fraction) and extrinsic factors (including density, average grain size, and phase composition) [44-45]. However, the quality factor (Q_f) exhibited a decline with increased doping, from 5229 for BVT to 5112 and 4463 for 1SBVT and 2SBVT, respectively, which indicates higher microwave losses due to increased structural imperfections and grain boundary effects.

The temperature coefficient of frequency (τ_f) values showed improvement with Sr doping, shifting from −134 ppm/°C for BVT to −118 ppm/°C and −110 ppm/°C for 1SBVT and 2SBVT, respectively. This reduction in the absolute TCF values suggests that strontium doping reduces thermal strain effects, thereby enhancing frequency stability. Strain analysis revealed an increase in strain with higher doping levels, while the grain size and crystalline size decreased. The reduced grain size contributes to additional grain boundaries, which are associated with increased microwave losses, as reflected in the declining quality factor values.

Similarly, X-ray diffraction (XRD) analysis revealed a decrease in crystalline size with Sr doping, likely due to restricted grain growth during the sintering process. The reduction in crystallite size, smaller particle dimensions, and increased strain will enhance polarization, which raises the dielectric constant. However, these changes also introduce defects and grain boundary conduction, contributing to higher dielectric loss. Additionally, the relative density of the samples improved significantly with doping, increasing from 88% for BVT to 94.6% for 1SBVT and 97.73% for 2SBVT. The increased relative densification will minimize porosity and enhance the polarization mechanics which tends to enhanced dielectric properties but also introduces microstructural changes that negatively affect the quality factor (Q_f). Overall, Sr doping in BVT ceramics enhances dielectric permittivity, make them ideal for applications in resonators, filters, antennas, and frequency-stable microwave devices.

4. Conclusion

The system $Bi_{(1-2/3x)}Sr_xVO_4$-TiO_2(x = 0, 0.1, 0.15) is successfully developed by the traditional solid-state method. The prepared composite materials are identified with two phases, confirmed by the powder x-ray diffraction. The SEM with EDX test used to understand the surface morphology and elemental composition of the prepared composite materials. The FT-Raman spectrum is further confirmed the elements present in the system. The dielectric constant of the prepared material is found to increase from 62 to 120 with the increase of strontium dopant concentration. The microwave dielectric permittivity (ε_r) improved significantly with doping, from 68 to 77. Also, the temperature coefficient of frequency (τ_f) is enhanced from −134 ppm/°C for BVT to −118 ppm/°C and −110 ppm/°C for the doped samples 1SBVT and 2SBVT respectively, demonstrating better frequency stability. These findings provide a pathway for optimizing these materials for use in resonators, filters, and frequency-stable microwave devices, contributing to advancements in communication and electronic systems.

Acknowledgement

Dr. N. Sivakumar and Dr. Ali Alsulmi acknowledge the Researchers Supporting Project (RSP2025R78), King Saud University, Riyadh, Saudi Arabia for the partial financial support. This work was partially carried out using the facilities of UGC-DAECSR. The authors acknowledge the financial support from UGC-DAE CSR through a Collaborative Research Scheme (CRS) with project number CRS/2021-22/04/627**.**

References

[1] Mailadil T. Sebastian "Dielectric materials for wireless communication" 2008.

[2] In-Young Kang, In-Tae Seo, Yu-Joung Cha, Jae-Hong Choi, Sahn Nahm, Tae Hyun Sung, Jong-Hoo Paik, J. Eur. Ceram. Soc., (2012) https://doi.org/10.1016/j.jeurceramsoc.2012.01.030

[3] Huanfu Zhou, Xiaobin Liu, Xiuli Chen, Liang Fang, Yiliang Wang J. Eur. Ceram. Soc., (2012) https://doi.org/10.1016/j.jeurceramsoc.2011.08.036

[4] Dong Zou, Qilong Zhang, Hui Yang, Shaochun Li J. Eur. Ceram Soc., (2008) https://doi.org/10.1016/j.jeurceramsoc.2008.04.021

[5] Y. Hyuk-Joon, S. Tomohiro, C.A. Rall, T.R. Shrout, M.T. Lanagan, J. Am. Ceram. Soc., (2001). https://doi.org/10.1111/j.1151-2916.2001.tb01053.x

[6] M.C. Wu, K.T. Huang, W.F. Su, Mater. Chem. Phys., (2006) https://doi.org/10.1016/j.matchemphys.2005.09.054

[7] C.L. Huang, M.H. Weng, Mater. Lett., (2000). https://doi.org/10.1016/S0167-577X(99)00226-8

[8] H.R. Lee, K.H. Yoon, E.S. Kim, Jpn. J. Appl. Phys., (2003). https://doi.org/10.1143/JJAP.42.6168

[9] A.W. Sleight, W.J. Linn, Ann. N. Y. Acad. Sci., (1976). https://doi.org/10.1111/j.1749-6632.1976.tb34222.x

[10] R.G.M. Oliveira, D.B. Freitas, G.S. Batista, J.E.V. de Morais, V.C. Martins, M.M. Costa, M.A.S. Silva, D.X. Gouvêa, C. Singh, A.S.B. Sombra, J. Mater. Sci.: Mater. Electron.,(2018). https://doi.org/10.1007/s10854-018-9714-8

[11] Lim AR, Choh SH, Jang MS., J Phys Condens Matter., (1995) https://doi.org/10.1088/0953-8984/7/37/005

[12] Pookmanee P, Kojinok S, Puntharod R, Sangsrichan S, Phanichphant S., Ferroelectrics, (2013). https://doi.org/10.1080/00150193.2013.846197

[13] Hirota K, Komatsu G, Yamashita M, Takemura H, Yamaguchi O., Mater. Res. Bull., (1992) https://doi.org/10.1016/0025-5408(92)90177-2

[14] Manolikas C, Amelinckx S., Phys Status Solidi, (1980) https://doi.org/10.1002/pssa.2210600120

[15] Yin W, Wang W, Zhou L, Sun S, Zhang L, J Hazard Mater, (2010) https://doi.org/10.1016/j.jhazmat.2009.08.068

[16] Guo YY, Yang X, Ma F, Li K, Xu L, Yuan X, Appl. Surf. Sci., (2010) https://doi.org/10.1016/j.apsusc.2009.09.076

[17] da Silva, M.R., Dall'Antonia, L.H., Scalvi, L.V.A., J Solid State Electrochem, (2012) https://doi.org/10.1007/s10008-012-1765-9

[18] D. Zhou, L.-X. Pang, J. Guo, H. Wang, X. Yao, C. Randall, ACS Pub. Inorg. Chem., (2011) https://doi.org/10.1021/ic201862e

[19] Zhou D, Pang L-X, Guo J, Qi Z-M, Shao T, Wang Q-P, Inorg Chem., (2014) https://doi.org/10.1021/ic402525w.

[20] J. H. Noh, H. S. Jung, J. K. Lee, J. R. Kim and K. S. Hong, J. Eur. Ceram. Soc., (2007) https://doi.org/10.1016/j.jeurceramsoc.2006.11.018

[21] R. G. M. Oliveira, D. C. Souza, J. E. V. de Morais, G. S. Batista, M. A. S. Silva, D. X. Gouveia, S. Trukhanov, A. Trukhanov, L. Panina, C. Singh, D. Zhou, A. S. B. Sombra J. Mater. Sci.: Mater. Electron., (2020) https://doi.org/10.1007/s10854-020-03858-x

[22] G.H. Chen, F.F. Gu, M. Pan, L.Q. Yao, M. Li, X. Chen, Y. Yang, T. Yang, C.L. Yuan, C.R. Zhou, J. Mater. Sci. .: Mater. Electron, (2015) https://doi.org/10.1007/s10854-015-3246-2

[23] R. G. M. Oliveira,G. S. Batista, J. E. V. de Morais, M. M. Costa, M. A. S. Silva, J. W. O. Bezerra, A.S.B. Sombra, J. Mater. Sci.: Mater. Electron, (2018) https://doi.org/10.1007/s10854-018-9590-2

[24] Peiwen Lv, Meng Zheng, Xian Wang, Feng Huang, J. Alloys and Compound,(2014). https://doi.org/10.1016/j.jallcom.2013.07.156

[25] Di Zhou, Dan Guo, Wen-Bo Li, Li-Xia Pang, Xi Yao, Da-Wei Wang and Ian M. Reaney J. Mater. Chem. C, (2016) https://doi.org/10.1039/C6TC01431C .

[26] P. Sakthivel, S. Muthukumaran, J. Inorganic Organoment. Polym. Mater., (2016) https://doi.org/10.1007/s10904-016-0341-7

[27] Manuel Ocaña, Jose V. Garcia-Ramos, Carlos J. Serna., J Am Ceram Soc, 75, (1992) 2010-12 https://doi.org/10.1111/j.1151-2916.1992.tb07237.x

[28] Ying Wang, Guoqiang Tan, Ting Liu, Yuning Su, Huijun Ren, XinLei Zhang, Ao Xia, Long Lv, Yun Liu, Appl. Catal. B Environ., (2018) https://doi.org/10.1016/j.apcatb.2018.04.026

[29] Vinothkumar, V., Sangili, A., Chen, S.-M., Abinaya, M. Colloids Surf. A Physicochem. Eng. Asp., (2021) https://doi.org/10.1016/j.colsurfa.2021.126849

[30] Thummala Jayalakshmi, Udayabhanu, and Ganganagappa Nagaraju J Mater Sci: Mater Electron (2023) https://doi.org/10.1007/s10854-023-10394-x

[31] J. Yoshino, N. Kano, T. Kawashima, J. Org. Chem., (2009) https://doi.org/10.1021/jo901733b

[32] N. Sudharsana, S. Muthunatesan, G. Jasmine Priya, V. Krishnakumar, R. Nagalakshmi,, Spectrochim. Acta, (2014) https://doi.org/10.1016/j.saa.2013.10.047Get rights and content

[33] Hoffart, L., Heider, U., Huggins, R.A Ionics, (1996) https://doi.org/10.1007/BF02375866

[34] Gu, Ff., Chen, Gh., Kang, Xl. J Mater Sci: Mater. Electron, (2015) https://doi.org/10.1007/s10853-014-8688-z

[35] D. Zhou, L.-X. Pang, H. Wang, J. Guo, X. Yao, C.A. Randall, J. Mater. Chem. (2011) https://doi.org/10.1039/C1JM14004C

[36] M.I.M.T. Abdullah, A. Halim, N.M. Ali, Malays. J. Anal. Sci. 13, 151 (2009).

[37] R.G.M. Oliveira, J.E.V. de Morais, G.S. Batista, M.A.S. Silva, J.C. Goes, A.S.B. Sombra," J. Alloys Compd., (2019) https://doi.org/10.1016/j.jallcom.2018.10.018

[38] R.G.M. Oliveira, R.A. Silva, J.E.V. de Morais, G.S. Batista, M.A.S. Silva, J.C. Goes, H.D. de Andrade, I.S. Queiroz Júnior, C. Singh, A.S.B. Sombra, Compos. B Eng., (2019). https://doi.org/10.1016/j.compositesb.2019.107122

[39] L.R. Dalton, J. Phys. Condens. Matter, (2003) DOI:10.1088/0953-8984/15/20/203

[40] N. Sivakumar, N. Kanagathara, G. Bhagavannarayana, S. Kalainathan, G. Anbalagan, J. Cryst. Growth, (2015) https://doi.org/10.1016/j.jcrysgro.2015.05.025

[41] E.I. Izgorodina, M. Forsyth, D.R. MacFarlane, Phys. Chem. Chem. Phys., (2009) http://dx.doi.org/10.1039/B815835E

[42] Jonscher A K "Universal Relaxation Law: A Sequel to Dielectric Relaxation in Solids" London: Chelsea Dielectrics Press, ISBN: 9780950871127 (1996)

[43] George S, Sebastian MT., J Am Ceram Soc, (2010) https://doi.org/10.1111/j.1551-2916.2010.03703.x

[44] Gurevich VL, Tagantsev AK., Adv Phys, (1991). https://doi.org/10.1080/00018739100101552

[45] Kangguo Wang, Huanfu Zhou, Xiaobin Liu, Wendong Sun, Xiuli Chen, Hong Ruan, J Eur Ceram Soc, (2019) https://doi.org/10.1016/j.jeurceramsoc.2018.12.059

Statements & Declarations

Funding

This work was partially supported by King Saud University under Researchers Supporting Project (RSP-R2024/78). Authors Dr. N. Sivakumar and Dr. Ali Alsulmi have received research support from King Saud University, Saudi Arabia under RPS Scheme. Also, financially supported by UGC-DAE CSR through a Collaborative Research Scheme (CRS) with project number CRS/2021-22/04/627

Competing Interests

Authors K. Yukesh Kumar, G.M. Bhalerao, G. Anbalagan and Kentaro Tashiro declare they have no financial interests. Authors Dr. N. Sivakumar and Dr. Ali Alsulmi have received research support from King Saud University, Saudi Arabia under RPS Scheme. Author Dr. N. Sivakumar received financial support from UGC-DAE CSR through a Collaborative Research Scheme (CRS).

Author Contributions

All authors contributed to the study conception and design. Material preparation was done by K. Yukesh Kumar. Data collection and analysis were performed by K. Yukesh Kumar. The first draft of the manuscript was written by N. Sivakumar and all the other authors commented on previous versions of the manuscript. Dr. Kentaro Tashiro supported for the dielectric interpretation. Finally it was validated by G.M. Bhalerao and G. Anbalagan. All authors read and approved the final manuscript.

Research Data Policy and Data Availability Statements

Data sharing not applicable to this article as no datasets were generated or analyzed during the current study.

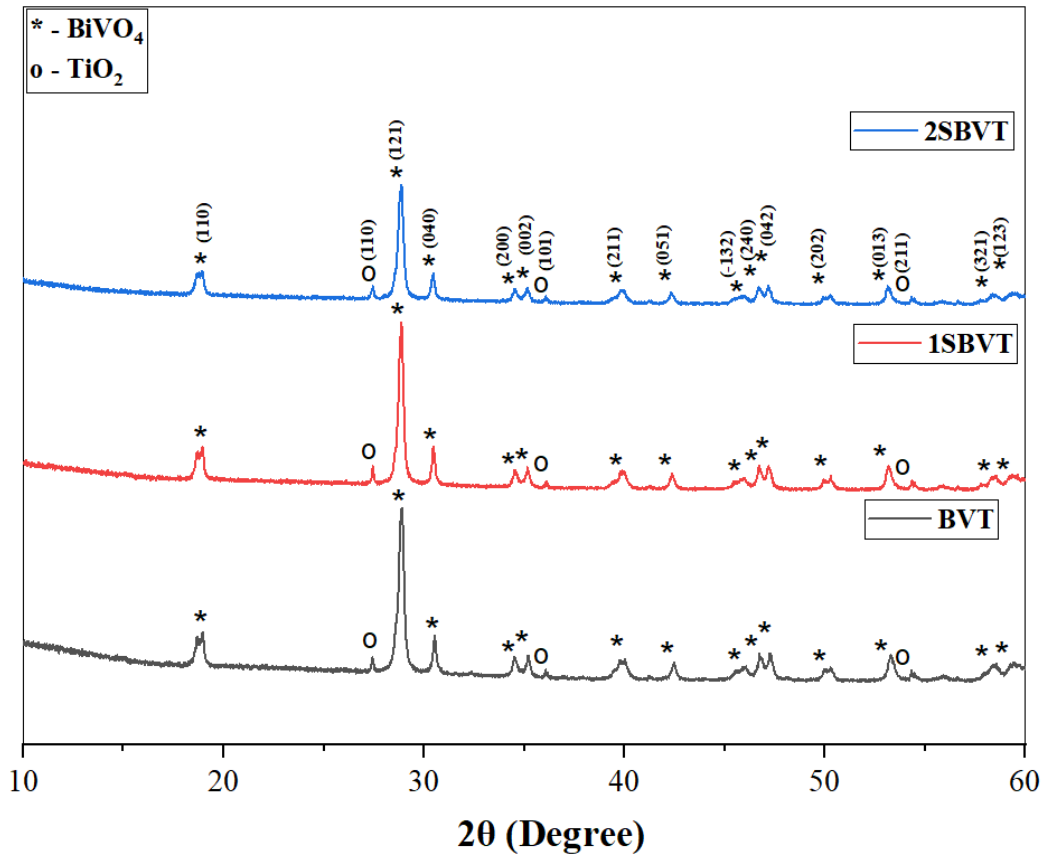

Fig.1. Powder XRD patterns of pure $BiVO_4$-TiO_2 (BVT), 0.1 wt% Sr doped (1SBVT) and 0.15 wt% Sr doped $BiVO_4$-TiO_2 (2SBVT) composite materials

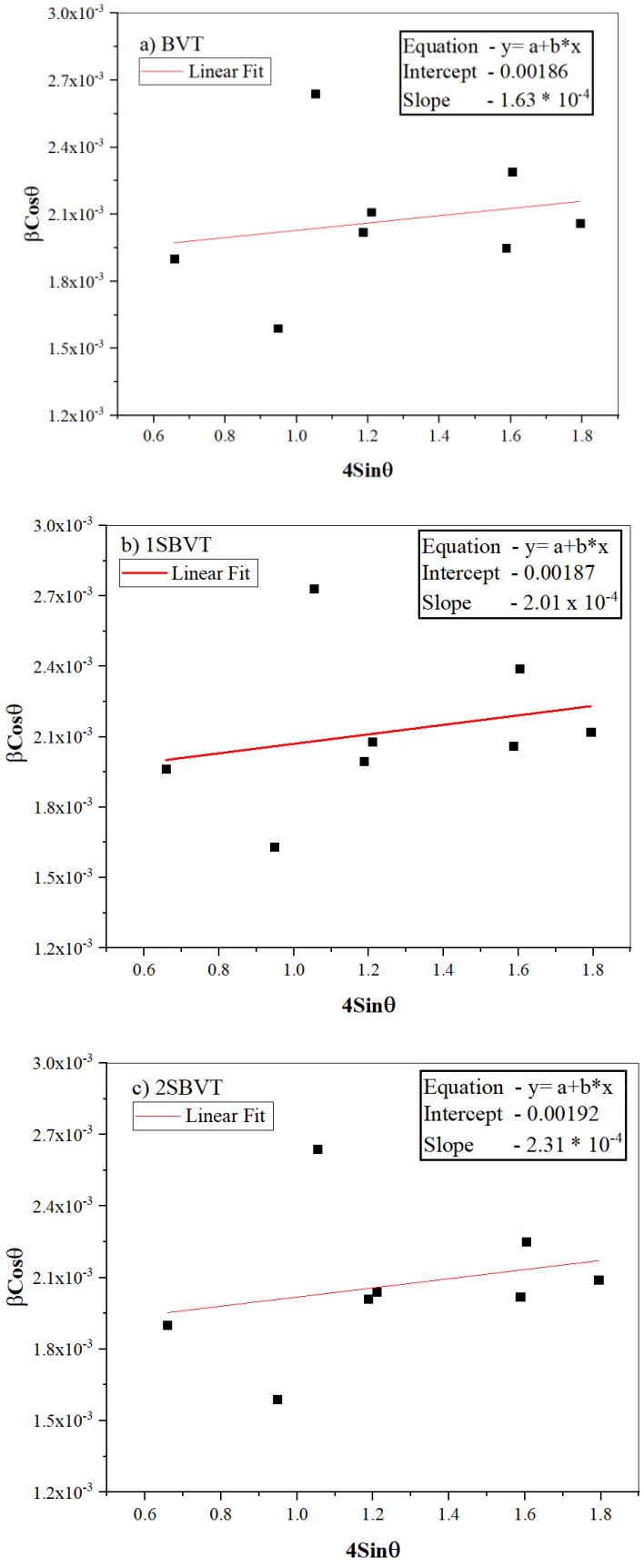

Fig.2. Williamson Hall of (a) pure $BiVO_4$-TiO_2, (b) 0.1 wt% Sr doped and (c) 0.15 wt% Sr doped $BiVO_4$-TiO_2 composite materials

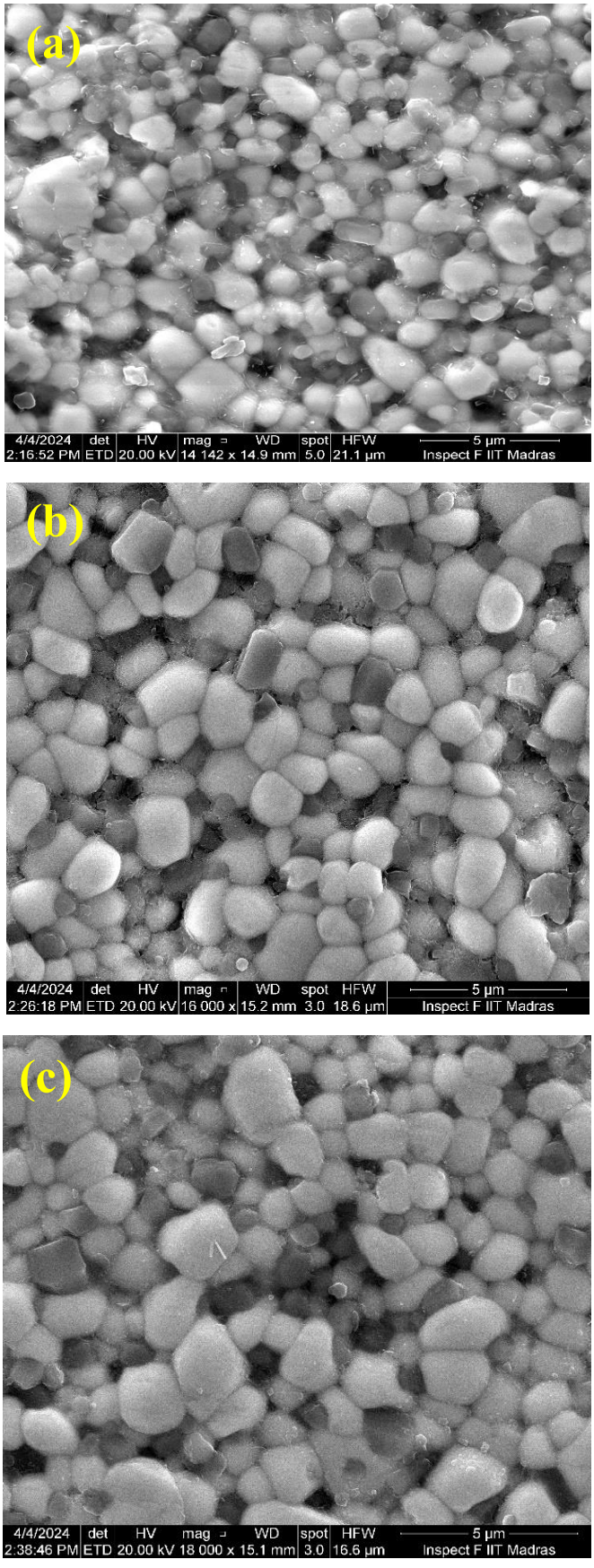

Fig. 3 FE-SEM images of (a) pure $BiVO_4$-TiO_2, (b) 0.1 wt% Sr doped and (c) 0.15 wt% Sr doped $BiVO_4$-TiO_2 composite materials

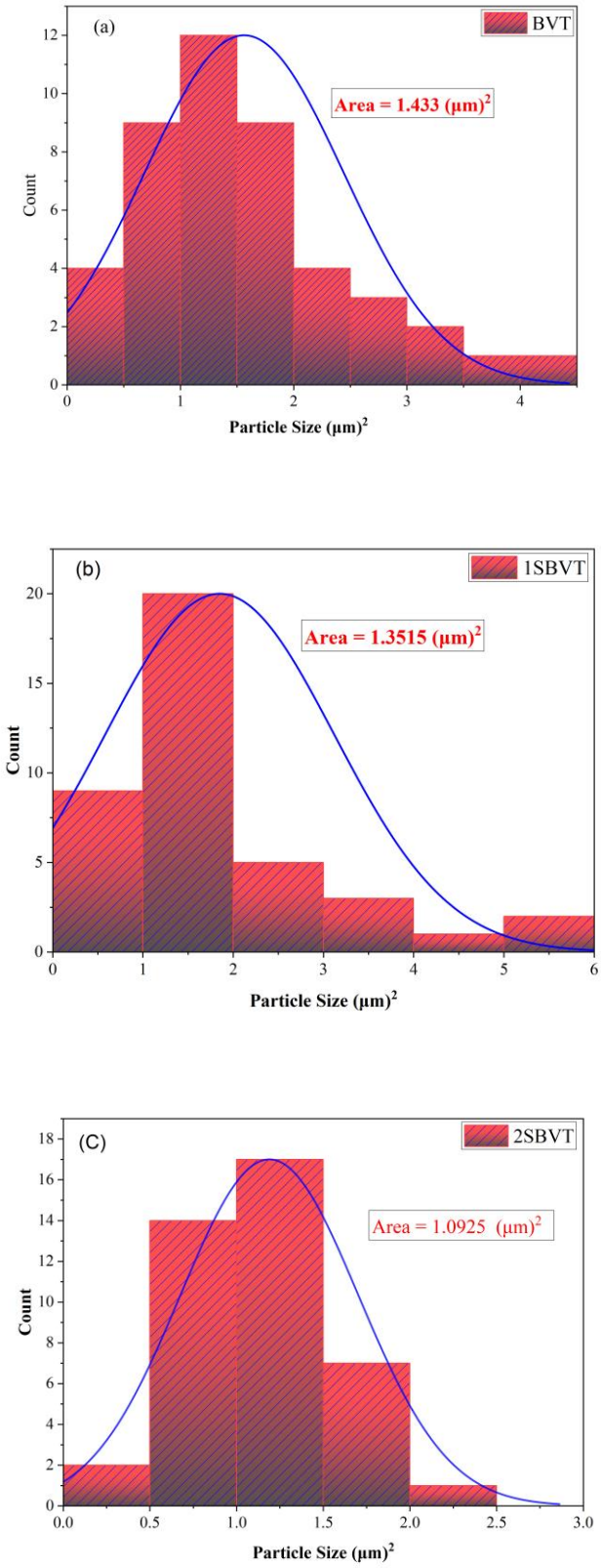

Fig. 4 Histogram grain size distribution of (a) pure $BiVO_4$-TiO_2, (b) 0.1 wt% Sr doped and (c) 0.15 wt% Sr doped $BiVO_4$-TiO_2 composite materials

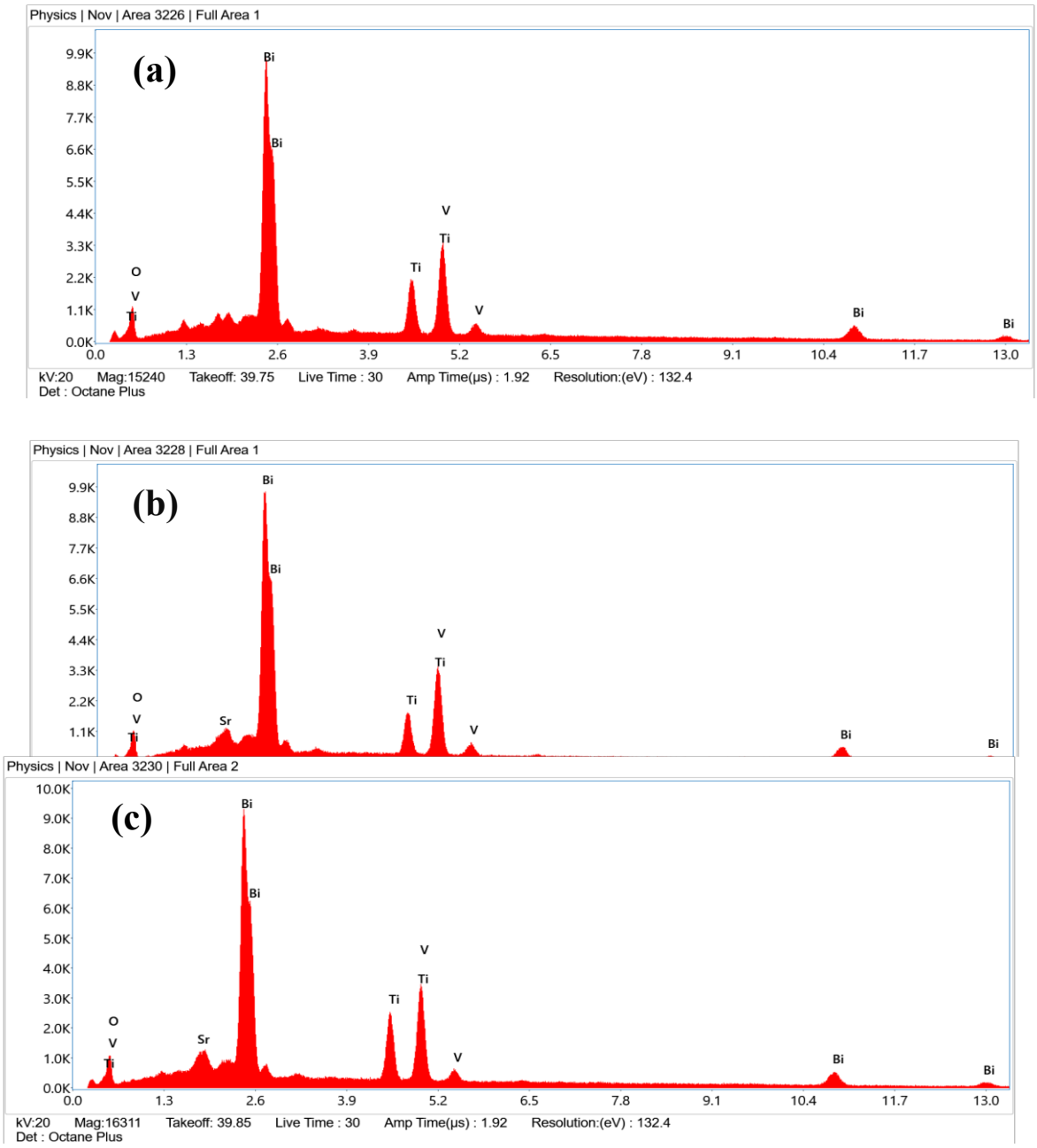

Fig. 5 EDX elemental compositional analysis of (a) pure $BiVO_4$-TiO_2, (b) 0.1 wt% Sr doped and (c) 0.15 wt% Sr doped $BiVO_4$-TiO_2 composite materials

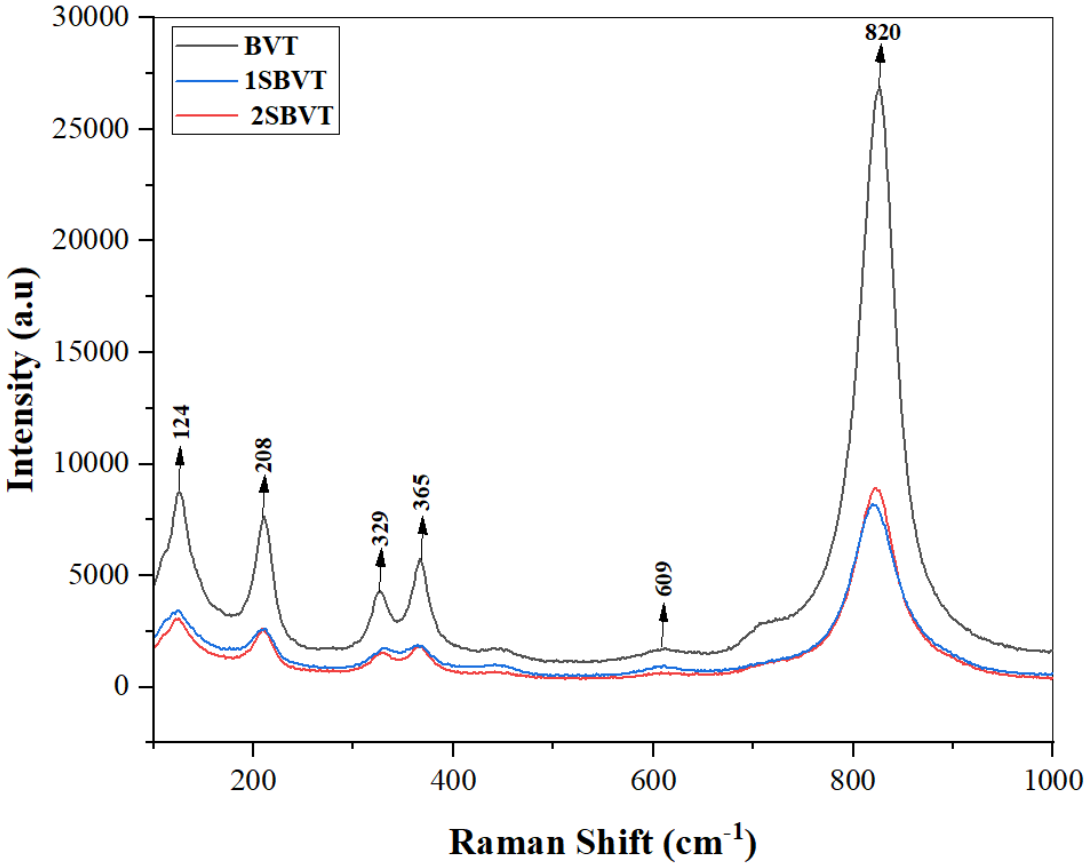

Fig. 6 FT-Raman spectra of pure $BiVO_4$-TiO_2 (BVT), 0.1 wt% Sr doped (1SBVT) and 0.15 wt% Sr doped $BiVO_4$-TiO_2 (2SBVT) composite materials

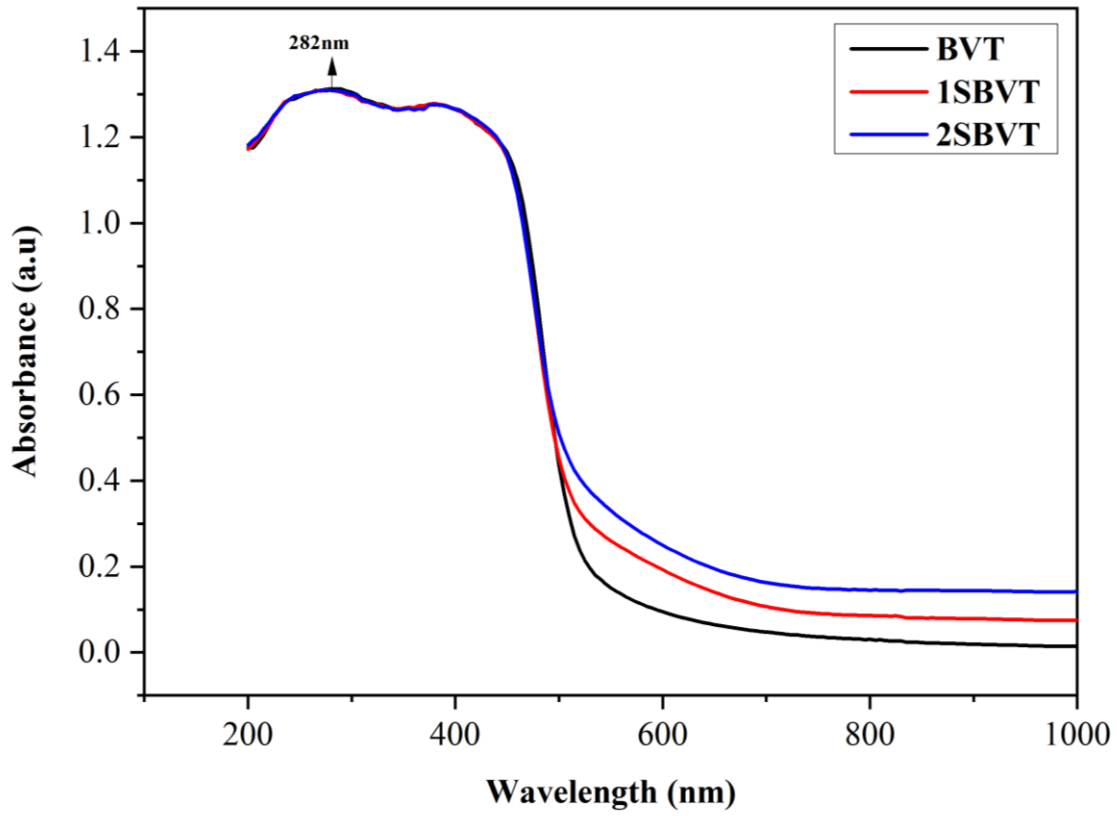

Fig. 7 UV Vis. absorbance spectra of pure $BiVO_4$-TiO_2 (BVT), 0.1 wt% Sr doped (1SBVT) and (c) 0.15 wt% Sr doped $BiVO_4$-TiO_2 (2SBVT) composite materials

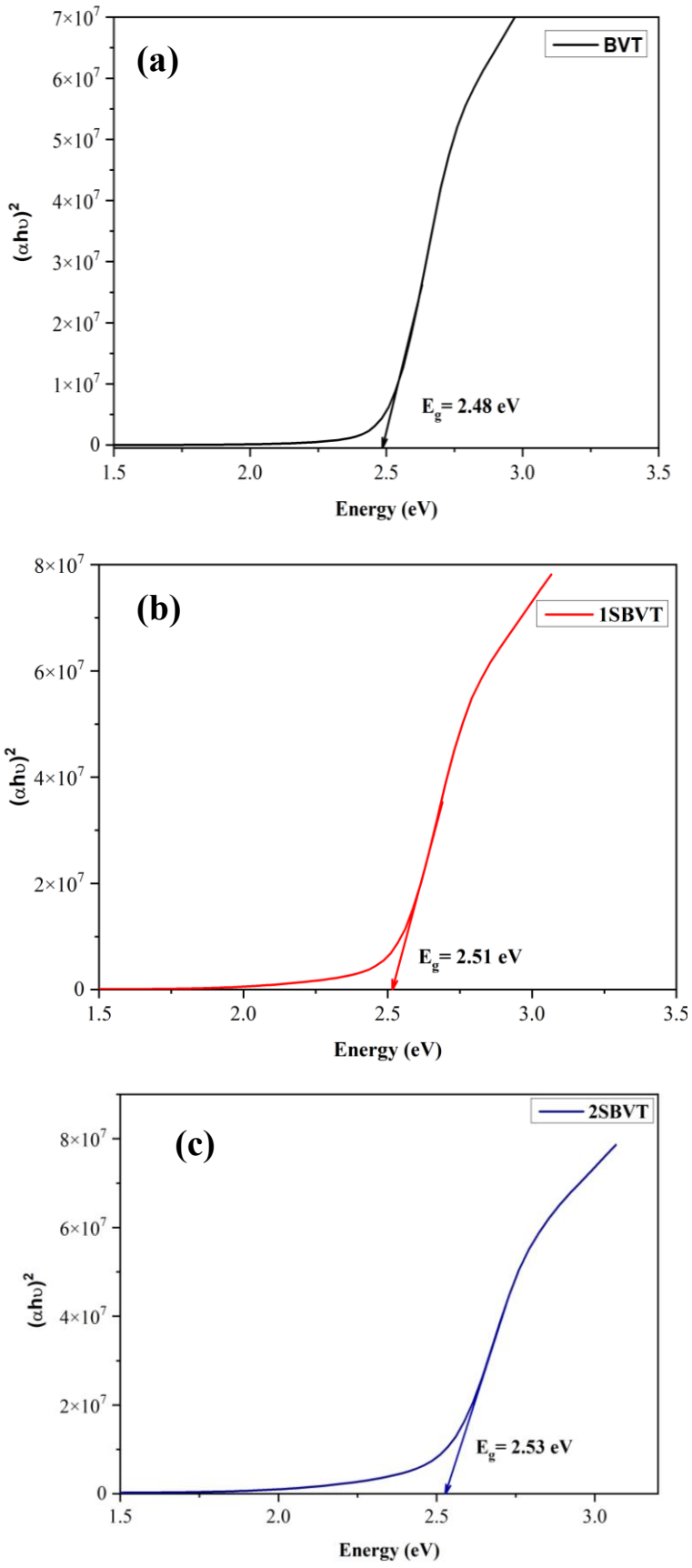

Fig. 8 Optical band gap of (a) pure $BiVO_4$-TiO_2 (BVT), (b) 0.1 wt% Sr doped (1SBVT) and (c) 0.15 wt% Sr doped $BiVO_4$-TiO_2 (2SBVT) composite materials

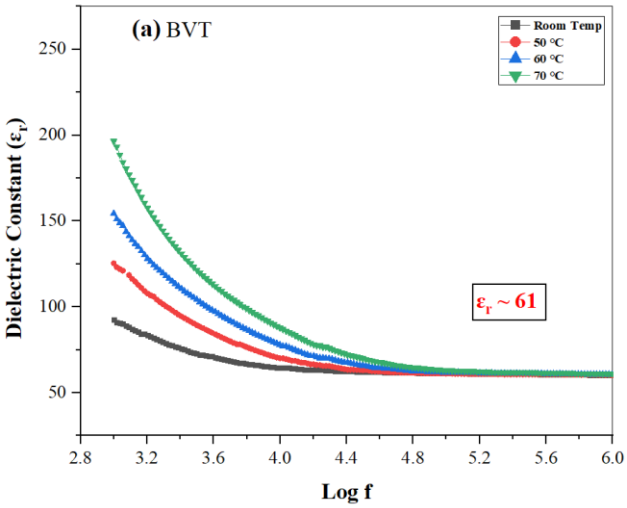

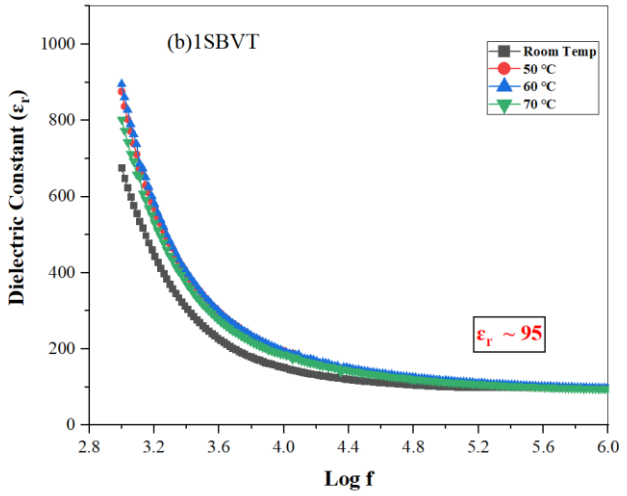

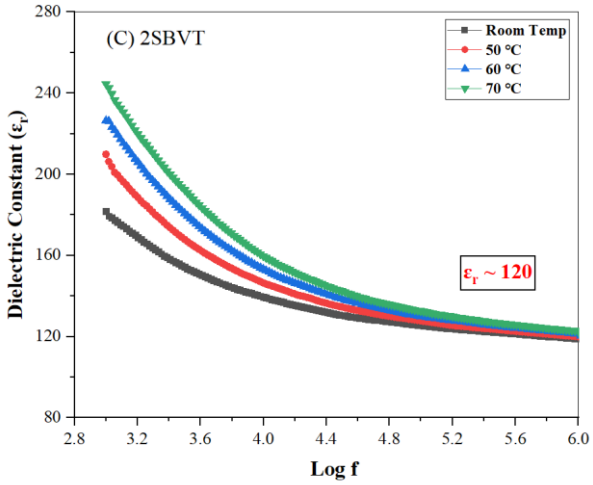

Fig. 9 Dielectric constant plots of (a) pure $BiVO_4$-TiO_2 (BVT), (b) 0.1 wt% Sr doped (1SBVT) and (c) 0.15 wt% Sr doped $BiVO_4$-TiO_2 (2SBVT) composite materials

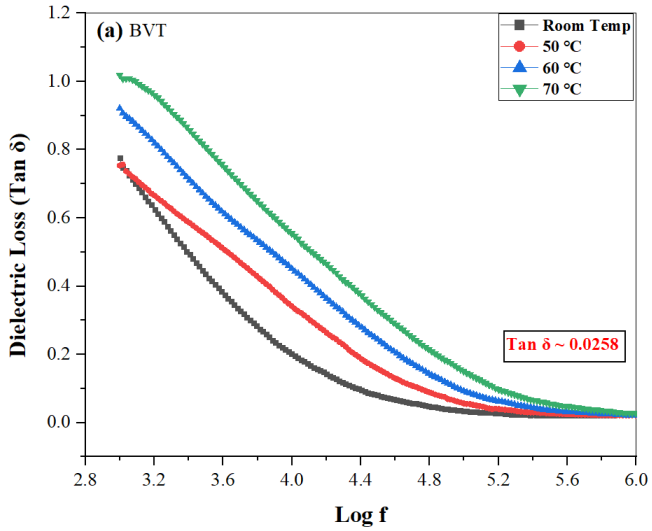

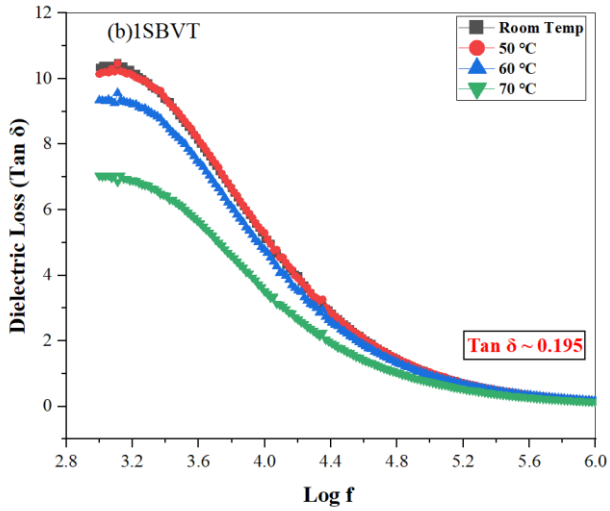

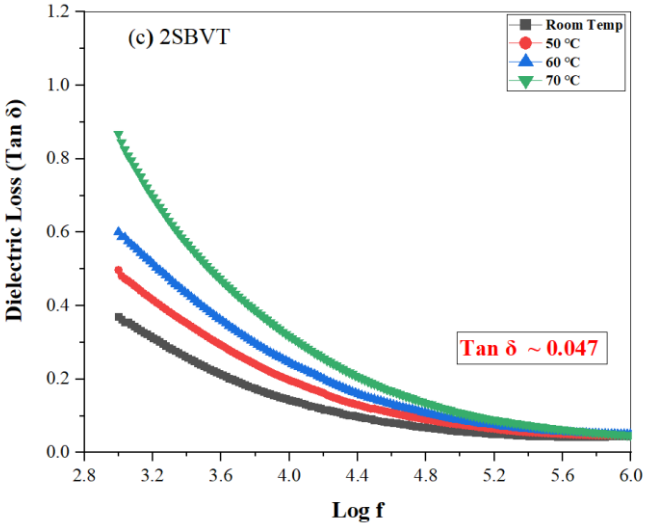

Fig. 10 Dielectric loss plots of (a) pure $BiVO_4$-TiO_2 (BVT), (b) 0.1 wt% Sr doped (1SBVT) and (c) 0.15 wt% Sr doped $BiVO_4$-TiO_2 (2SBVT) composite materials

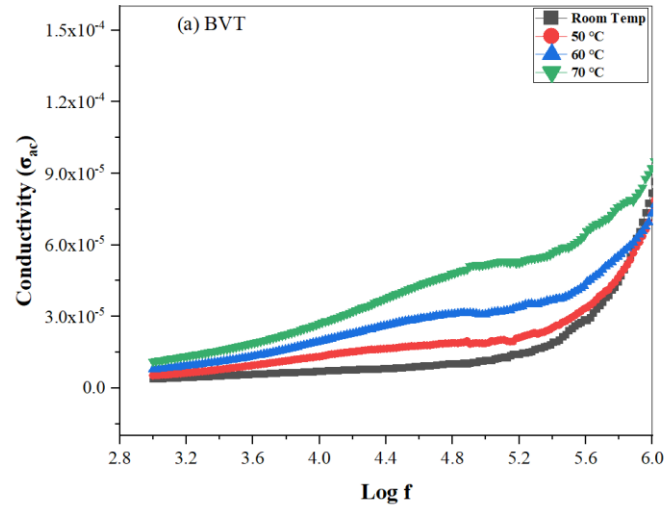

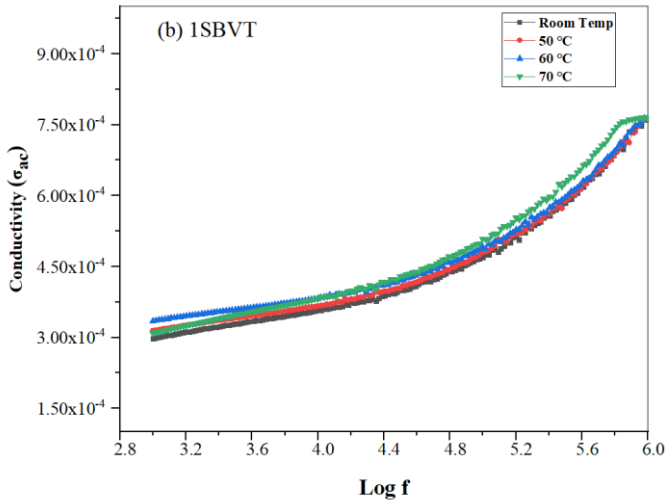

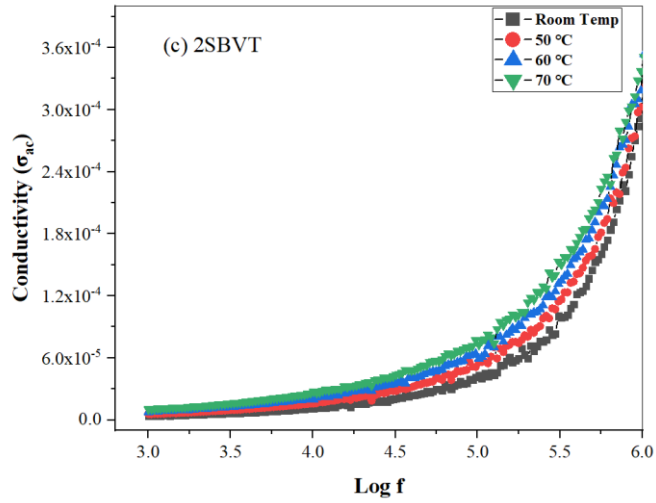

Fig. 11 Electrical Conductivity plots of (a) pure $BiVO_4$-TiO_2 (BVT), (b) 0.1 wt% Sr doped (1SBVT) and (c) 0.15 wt% Sr doped $BiVO_4$-TiO_2 composite materials

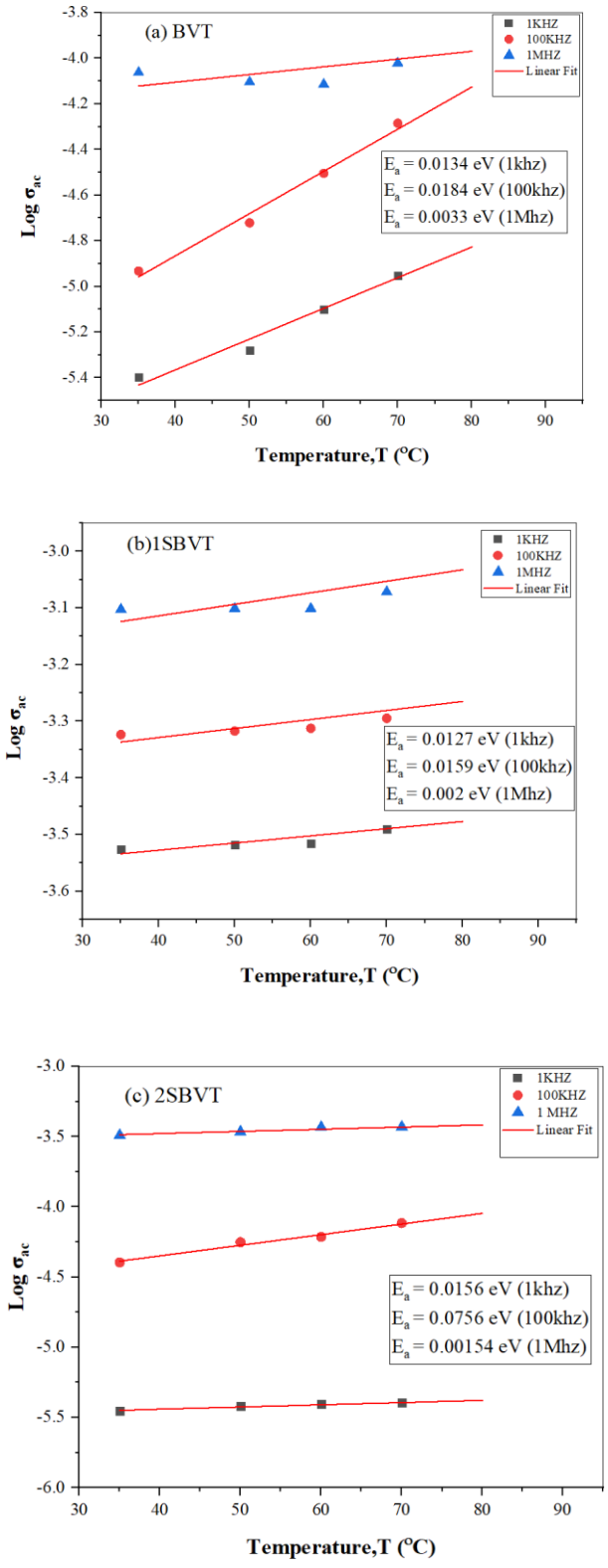

Fig. 12 Activation energy E_a plots of (a) pure $BiVO_4$-TiO_2 (BVT), (b) 0.1 wt% Sr doped (1SBVT) and (c) 0.15 wt% Sr doped $BiVO_4$-TiO_2 composite materials

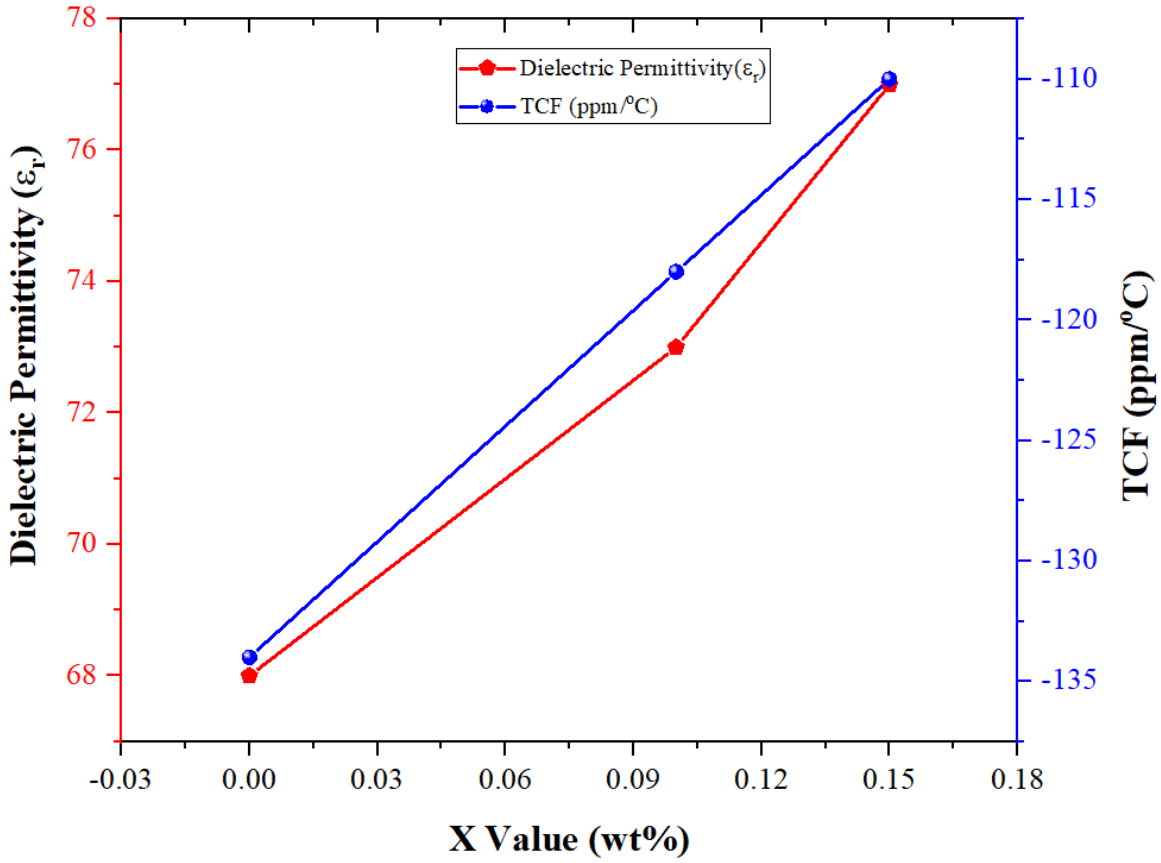

Fig.13 Dielectric permittivity and Temperature Co-efficient resonant frequency of pure $BiVO_4$-TiO_2 (BVT), 0.1 wt% Sr doped (1SBVT) and 0.15 wt% Sr doped $BiVO_4$-TiO_2 composite materials

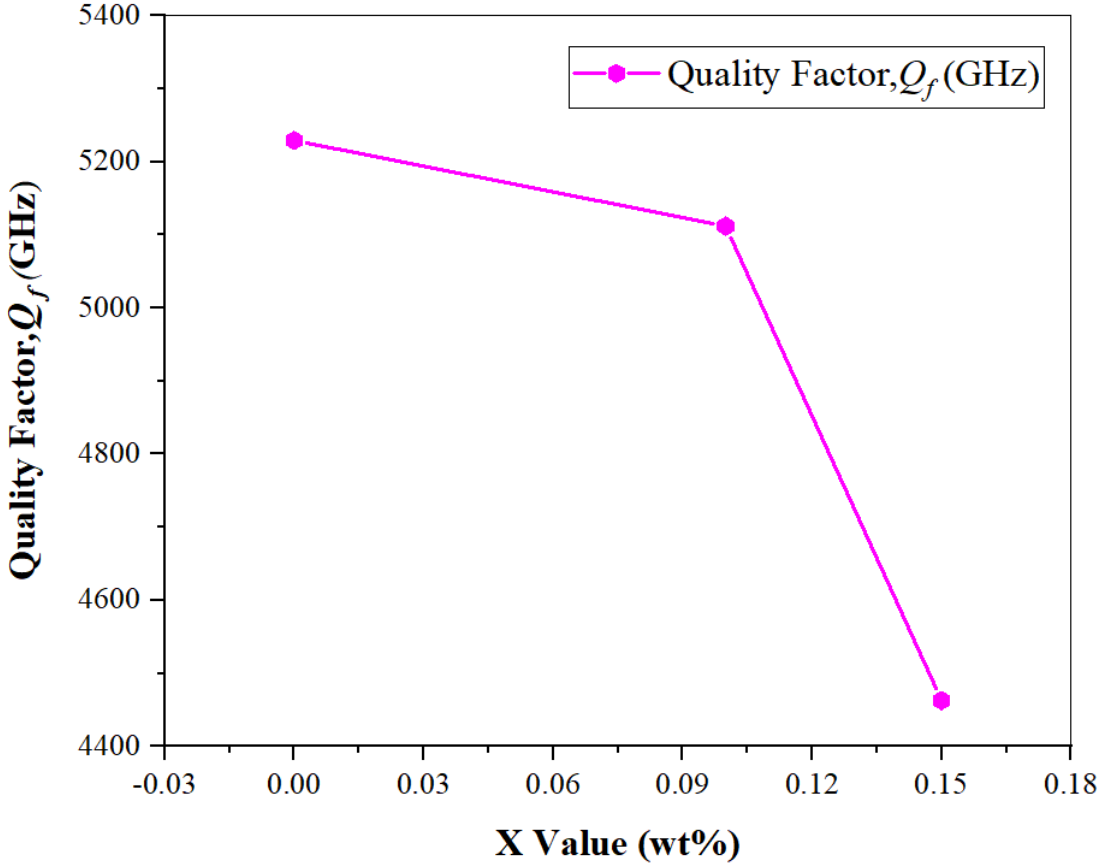

Fig. 14 Quality factor of pure $BiVO_4$-TiO_2 (BVT), 0.1 wt% Sr doped (1SBVT) and (c) 0.15 wt% Sr doped $BiVO_4$-TiO_2 composite materials

Table 1:

Weight percentage of the chemical elements of pure $BiVO_4$-TiO_2 (BVT), 0.1 wt% Sr doped (1SBVT) and (c) 0.15 wt% Sr doped $BiVO_4$-TiO_2 composite materials.

Element	BVT Weight %	1SBVT Weight %	2SBVT Weight %
Bi	60.7 ± 0.32	58.9 ± 0.45	58.4 ± 0.48
V	14.3 ± 0.25	14.1 ± 0.25	14.8 ± 0.33
O	12.8 ± 0.61	11.4 ± 0.84	10.7 ± 0.83
Ti	12.2 ± 0.16	10.5 ± 0.33	10.3 ± 0.23
Sr	-	4.6 ± 0.04	5.8 ± 0.08

Table 2:

Raman vibrational assignments of pure $BiVO_4$-TiO_2 (BVT), 0.1 wt% Sr doped (1SBVT) and (c) 0.15 wt% Sr doped $BiVO_4$-TiO_2 composite materials.

Peak Positions (cm^{-1})	Assignment

124	O-Ti-O
208	Bi-O
329	Symmetrical of VO^{4+}
365	Asymmetrical bending mode of VO^{4+}
609	γ (O-Ti-O)
820	V-O